Development of a Panel Method for Preliminary Design of Aero-Propulsive Systems

Hemant Bommidala, Edgar Zambrano, Aleksandar Joksimović, Vincent Maillet, Xavier Carbonneau

Association Aéronautique et Astronautique de France

56th 3AF International Conference on Applied Aerodynamics
28 — 30 March 2022, Toulouse – France

FP94-2022-joksimovic

DEVELOPMENT OF A PANEL METHOD FOR PRELIMINARY DESIGN OF AERO-PROPULSIVE SYSTEMS

Hemant Bommidala[(1)], Edgar Zambrano [(1)], Aleksandar Joksimović[(1)], Vincent Maillet [(1)] and Xavier Carbonneau [(1)]
[(1)]ISAE-SUPAERO, Université de Toulouse, France, email: aleksandar.joksimovic@isae-supaero.fr

ABSTRACT

The paper presents development of a low-fidelity tool capable of calculating pressure and velocity field of an aero-propulsive element (aerofoil and an integrated ducted propulsor). To that end, conventional panel method is extended by including the emanating propulsive jet as a part of the solid aero-propulsive geometry. The mathematical formulations and the algorithm used by the tool to characterise the propulsor and determine the jet shape are presented. Then, a series of results and parametric studies performed with the tool considering different input parameters are shown in order to demonstrate the potential of the tool to tackle a broad design space. Rudimentary validation is carried out by comparing the calculated lift coefficient at different angles of attack is compared with reference RANS CFD results; agreement between the two is observed, especially at low angles of attack.

1. INTRODUCTION

Civil aviation is currently estimated to contribute around 5% of the total anthropogenic impact [1] to the radiative forcing. Rethinking whole airplane architectures and configurations thereof is in focus as a pathway to rendering the global industry compatible with environmental sustainability goals. This paper focuses on the innovative aeroplane concept subspace based on airframe-propulsive system synergies, in particular on concepts that employ propulsion distribution [2]. Such forms rely on reducing the airplane mission energy requirements (and thus the emissions) by redistributing thrust across the airframe in order to seek higher vehicle-level efficiency. The sheer number of possible solutions still poses an important challenge in conceptual design decision-making process. One prominent subset of the aero-propulsive concept space explored previously at ISAE-SUPAERO is Boundary Layer Ingestion (BLI). [3] A review of BLI modelling methods assembled by Hendricks [4] provides a useful insight that there are comparatively few methods to model BLI which fully couple external aerodynamics and propulsion. Moreover, analysis often relies on full CFD, which is computationally expensive in the context of conceptual design decision making.

The objective of the presented work is therefore to develop a low-order tool for identifying performance tendencies of aero-propulsive concepts within this vast design space by providing insight into correlations between propulsive power and aerodynamic performance for various geometries and at various operating conditions. The results can be used to robustly initialise preliminary design calculations that require more computationally expensive high-fidelity tools such as previously used by the authors, as presented in [3].

Further literature survey revealed previous works which ventured to use panel method modelling to provide simple models of specific aero-propulsive configurations. Albers [5] carried out an analysis of two dimensional wing-fan system which consists of aerofoil with flaps, fans, distributed suction at the inlet and a jet sheet leaving from the flap trailing edge, for providing an incompressible potential flow solution using panel methods. Spence [6] carried out analysis for an inviscid, incompressible flow for jet flapped aerofoils at low angles of attack by bounding the exhaust jet by vortex sheets to prevent its mixing with the main stream, with an experimental validation of the obtained results. This approach was a precise fit for the identified need for a tool to provide desired transparency of the possible aero-propulsive architectural space without resorting to computationally expensive modelling. An attempt was thus made to create a tool which would generalise the approach presented in the outlined references. For the time being, and throughout this paper, the work is constrained to two-dimensional analysis. To emphasise the contrast between the size

of aero-propulsive design space and the computational time/power limits, the interested reader is referred to one such design space exploration by Wick et al. [7], carried out by employing 2D CFD modelling.

The paper is structured as follows: Section 2 lays out the basic principles behind the panel-method modelling at hand; Section 3 breaks down the assumptions and modelling approach; Section 4 provides the preliminary results obtained by the developed tool, and Section 5 provides provisional conclusions and comments on further work.

2. AERO-PROPULSIVE SYSTEM

This work defines an aero-propulsive system as an integral element composed of an airframe part and a propulsor and which can be expressed in multiple distinct configurations (e.g. blown wing or BLI on the suction or pressure surface, see [7]). Following the approach presented by Albers [5] (cf. Section 3 for more details), the physical aero-propulsive geometry is complemented with a fictitious geometrical element representing the jet emanating from the system, which contributes to the overall aero-propulsive performance of the system. The equivalent body surface over which the potential flow is calculated is illustrated schematically in Fig. 1.

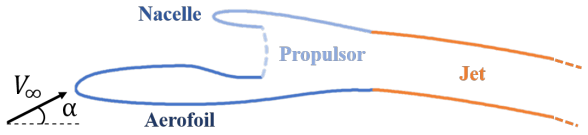

Figure 1: Elementary two-dimensional aero-propulsive system schematic overview.

The jet stream as it exits from the propulsor is at a higher total pressure than the surrounding fluid. For a portion of the exhaust jet the total pressure will be constant before undergoing a reduction in total pressure due increasingly important jet entrainment and mixing losses [5] and [8]. This portion of the exhaust jet and the aerofoil body are considered to be a part of the lifting surface in the developed model. Depending on the various flight conditions and propulsor power settings, the shape of this free jet is evaluated (details presented in subsection 3.4). The potential flow resolution for a defined configuration thus means calculating the velocity field on and external to the body for the combination of the following variables:

1. Free-stream velocity (V_∞),
2. Fan mass flow rate per unit span ($\dot{m}$),
3. Propulsive system thrust per unit span (T),
4. Flap angle (θ),
5. Wing angle of attack (α).

The jet emanating from the propulsive element at a velocity V_{jet} and an angle θ_{jet} is included in the model as this allows to capture a pressure rise in the flow field. The propulsor (with the emanating jet) and the aerodynamic element are considered as a unified solid body, i.e. there is no flow entering or leaving through the surfaces and there is no mixing of the jet stream with the free stream.

As explained previously, this work attempts to employ panel method modelling. As in the traditional approaches for external flow field calculation, the body of interest is discretised into as a series of panel sheets where elementary flows and boundary conditions are imposed in such way that the body itself acts as a streamline. In the work presented in this paper, the modelled body is not a simple closed-contour aerofoil, but a complex shape which ingests a part of the external flow. The next section presents the underlying details.

3. DEVELOPMENT OF THE TOOL

The following sections provide the relevant elaboration of the different modules involved in the panel code developed for purpose of two-dimensional aero-propulsive design space exploration.

3.1 Mathematical Formulations for Higher Order Panel Methods

Three different types of elementary flow distributions have been considered in the current work:

1. Discrete source panel distribution,
2. Quadratic source panel distribution,
3. Linear vortex panel distribution.

Fig. 2 presents the nomenclature used for the representation of panel sheets. For a sheet of elementary flows, the i^{th} panel between two nodal points given by (x_i, y_i) and (x_{i+1}, y_{i+1}) is characterised by the set of geometrical properties $(\delta_i, \phi_i, \beta_i, s_i)$ evaluated at the panel control point (X_i, Y_i). If s is the distance measured measured along the sheet in an edge view, the function $\lambda = \lambda(s)$ or $\gamma = \gamma(s)$ represents the source or vortex strength per unit length of the panel with an order $\mathcal{O}(\lambda(s))$ *or* $\mathcal{O}(\gamma(s)) = 0, 1, 2$, depicting a discrete, linear and quadratic strength variation of the elementary flows, respectively.

3.1.1 Discrete source panel distribution

An i^{th} discrete source panel has a constant source strength distribution per unit length ($\lambda(s) = \lambda_i$). The normal and tangential velocities $(V_{n,i}, V_{t,i})$ induced at control point of

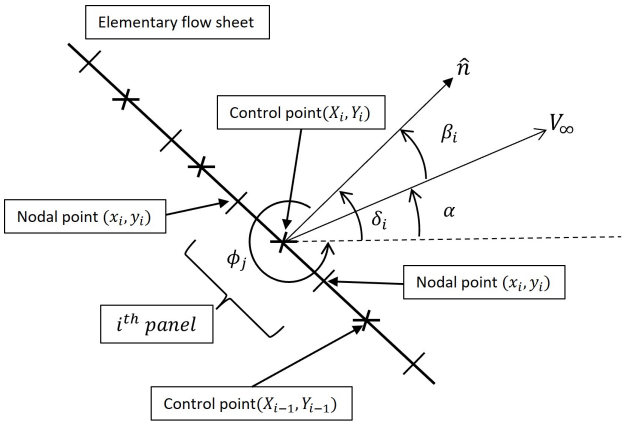

Figure 2: Panel geometric properties.

i^{th} panel due N similar panels are written as

$$V_{n,i} = V_\infty \cos\beta_i + \sum_{j=1}^{N} \frac{\lambda_j}{2\pi} an_{i,j} \tag{1}$$

$$V_{t,i} = V_\infty \sin\beta_i + \sum_{j=1}^{N} \frac{\lambda_j}{2\pi} at_{i,j} \tag{2}$$

$$an_{i,j} = an_{i,j}(x_i, y_i, X_j, Y_j, \phi_i, \phi_j, s_j)$$
$$at_{i,j} = at_{i,j}(x_i, y_i, X_j, Y_j, \phi_i, \phi_j, s_j)$$

where the functions $an_{i,j}$ and $at_{i,j}$ are referred from [9].

3.1.2 Quadratic source panel distribution

For any i^{th} quadratic source panel, the source strength per unit length varies as a quadratic function of distance s measured along the panel

$$\lambda(s) = a_q s^2 + b_q s + c_q$$

The normal and tangential velocities $(V_{n,i}, V_{t,i})$ induced at control point of i^{th} panel due N similar panels are written as

$$V_{n,i} = V_\infty \cos\beta_i + \sum_{j=1}^{n} \left(\frac{\lambda_{j+1}}{2\pi} An_{i,j} + \frac{\lambda_{j+\frac{1}{2}}}{2\pi} Bn_{i,j} + \frac{\lambda_j}{2\pi} Cn_{i,j} \right)$$

$$V_{t,i} = V_\infty \sin\beta_i + \sum_{j=1}^{n} \left(\frac{\lambda_{j+1}}{2\pi} At_{i,j} + \frac{\lambda_{j+\frac{1}{2}}}{2\pi} Bt_{i,j} + \frac{\lambda_j}{2\pi} Ct_{i,j} \right)$$

$$An_{i,j},\ Bn_{i,j},\ Cn_{i,j} = f_n(x_i, y_i, X_j, Y_j, s_j, \phi_i, \phi_j)$$

$$At_{i,j},\ Bt_{i,j},\ Ct_{i,j} = f_t(x_i, y_i, X_j, Y_j, s_j, \phi_i, \phi_j)$$

where λ_i, λ_{i+1} are the source strength per unit length at panel control points and $\lambda_{i+\frac{1}{2}}$ is the source strength per unit length at panel control point and the functions f_n and f_t are derived using similar methodologies used for discrete source panel methods described in [9].

3.1.3 Linear vortex panel distribution

For any i^{th} linear vortex panel, the vortex strength per unit length varies as a linear function of distance s measured along the panel

$$\gamma(s) = a_l s + b_l$$

The normal and tangential velocities $(V_{n,i}, V_{t,i})$ induced at control point of i^{th} panel due N similar panels are written as

$$V_{n,i} = V_\infty \cos\beta_i + \sum_{j=1}^{N} \left(\frac{\gamma_j}{2\pi} Dn_{i,j} + \frac{\gamma_{j+1}}{2\pi} En_{i,j} \right) \tag{3}$$

$$V_{t,i} = V_\infty \sin\beta_i + \sum_{j=1}^{N} \left(\frac{\gamma_j}{2\pi} Dt_{i,j} + \frac{\gamma_{j+1}}{2\pi} Et_{i,j} \right) \tag{4}$$

$$Dn_{i,j},\ En_{i,j} = g_n(x_i, y_i, X_j, Y_j, s_j, \phi_i, \phi_j)$$

$$Dt_{i,j},\ Et_{i,j} = g_t(x_i, y_i, X_j, Y_j, s_j, \phi_i, \phi_j)$$

where γ_i, γ_{i+1} are the vortex strength per unit length at panel control points and the function g_n and g_t are derived using the similar methodologies used for discrete vortex panel methods described in [9].

3.2 Panel Method Implementation for the Aero-Propulsive Element

The current configuration is summarised schematically in Fig. 3. The base aerofoil, nacelle aerofoil, upper jet, lower jet, velocity inlet and velocity outlet surfaces of the composite body are discretised into n_{base}, $n_{nacelle}$, n_{upper}, n_{lower}, n_{inlet} and n_{outlet} panels respectively. The resulting total number of panels then amounts to

$$n_{total} = n_{base} + n_{nacelle} + n_{upper} + n_{lower} + n_{inlet} + n_{outlet} \tag{5}$$

Base aerofoil, nacelle aerofoil, upper and lower jet surfaces are described using linear vortex panels, which requires $(n_{lower} + n_{base} + n_{nacelle} + n_{upper} + 2)$ variables to describe the panel's vortex strength. Velocity inlet and velocity outlet surfaces are described using quadratic source panels, which requires $(2(n_{inlet} + n_{outlet}) + 2)$ variables to describe the panel's vortex strength.

The total number of variables required for the inviscid flow field calculation are:

$$VAR_{count} = n_{lower} + n_{base} + n_{nacelle} + n_{upper} + 2(n_{outlet} + n_{inlet}) + 4 \tag{6}$$

From the mathematical formulations for the elementary flows derived in Section 3.1, the normal/tangential velocity induced at the control point of the i^{th} panel by all the remaining panels is given as

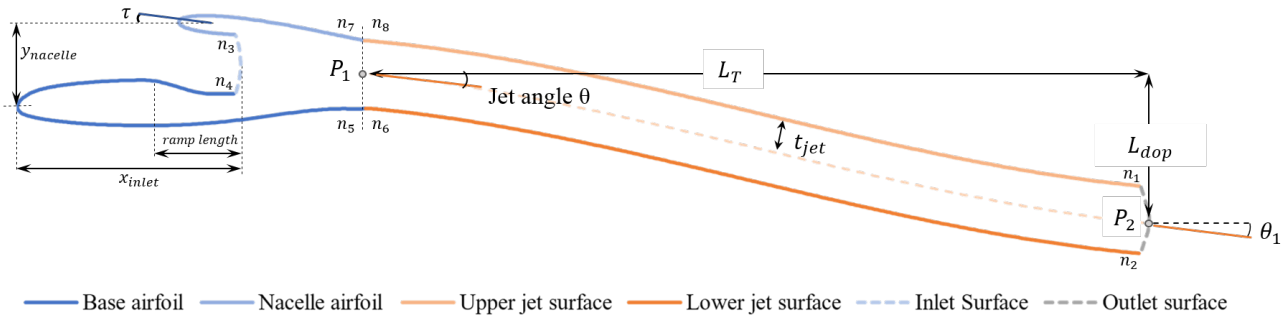

Figure 3: Elementary aero-propulsive configuration description and parametrisation.

$$
\begin{aligned}
V_{n,i} = V_\infty \cos\beta_i + &\sum_{j=1}^{n_{lower}+n_{base}} \left(\frac{\gamma_j}{2\pi} Dn_{i,j} + \frac{\gamma_{j+1}}{2\pi} En_{i,j}\right) \\
&+ \sum_{j=1}^{n_{outlet}} \left(\frac{\lambda_{j+1}}{2\pi} An_{i,j} + \frac{\lambda_{j+\frac{1}{2}}}{2\pi} Bn_{i,j} + \frac{\lambda_j}{2\pi} Cn_{i,j}\right) \\
&+ \sum_{j=1}^{n_{nacelle}+n_{upper}} \left(\frac{\gamma_j}{2\pi} Dn_{i,j} + \frac{\gamma_{j+1}}{2\pi} En_{i,j}\right) \\
&+ \sum_{j=1}^{n_{inlet}} \left(\frac{\lambda_{j+1}}{2\pi} An_{i,j} + \frac{\lambda_{j+\frac{1}{2}}}{2\pi} Bn_{i,j} + \frac{\lambda_j}{2\pi} Cn_{i,j}\right)
\end{aligned}
\tag{7}
$$

$$
\begin{aligned}
V_{t,i} = V_\infty \cos\beta_i + &\sum_{j=1}^{n_{lower}+n_{base}} \left(\frac{\gamma_j}{2\pi} Dt_{i,j} + \frac{\gamma_{j+1}}{2\pi} Et_{i,j}\right) \\
&+ \sum_{j=1}^{n_{outlet}} \left(\frac{\lambda_{j+1}}{2\pi} At_{i,j} + \frac{\lambda_{j+\frac{1}{2}}}{2\pi} Bt_{i,j} + \frac{\lambda_j}{2\pi} Ct_{i,j}\right) \\
&+ \sum_{j=1}^{n_{nacelle}+n_{upper}} \left(\frac{\gamma_j}{2\pi} Dt_{i,j} + \frac{\gamma_{j+1}}{2\pi} Et_{i,j}\right) \\
&+ \sum_{j=1}^{n_{inlet}} \left(\frac{\lambda_{j+1}}{2\pi} At_{i,j} + \frac{\lambda_{j+\frac{1}{2}}}{2\pi} Bt_{i,j} + \frac{\lambda_j}{2\pi} Ct_{i,j}\right)
\end{aligned}
\tag{8}
$$

This calls for the development of a system of equations of the same size as that of the VAR_{count}. The following boundary conditions are utilised:

1. Zero normal velocity at the control points of the panels located on base and nacelle aerofoil surface, upper and lower jet surface:

$$V_{n,i} = 0 \tag{9}$$

where i corresponds to the panels located on the surfaces mentioned earlier and this boundary condition results in a total of $(n_{lower} + n_{base} + n_{nacelle} + n_{upper})$ number of equations.

2. Velocity inlet boundary conditions on the inlet surface:

$$V_{x,i} = -V_{n,i}\sin\phi_i + V_{t,i}\cos\phi_i = V_{inlet,i} \tag{10}$$

$$V_{y,i} = -V_{n,i}\cos\phi_i + V_{t,i}\sin\phi_i = 0 \tag{11}$$

where i corresponds to the panels located on the velocity inlet surface. The velocity $(V_{inlet,i} = V_{prop,inlet})$ is calculated from the propulsor operating conditions with an assumption of a uniform inlet velocity distribution across the inlet surface. This boundary condition results in a total of $2\,(n_{inlet})$ number of equations.

3. Velocity outlet boundary conditions on the outlet surface:

$$
\begin{aligned}
V_{x,i} &= -V_{n,i}\sin\phi_i + V_{t,i}\cos\phi_i \\
&= V_{jet,i}\cos(\theta_1 + \alpha)
\end{aligned}
\tag{12}
$$

$$
\begin{aligned}
V_{y,i} &= -V_{n,i}\cos\phi_i + V_{t,i}\sin\phi_i \\
&= V_{jet,i}\sin(\theta_1 + \alpha)
\end{aligned}
\tag{13}
$$

where i corresponds to the panels located on the velocity outlet surface. The velocity $(V_{jet,i} = V_{prop,outlet})$ is calculated from the propulsor operating conditions and with an assumption of negligible drop in outlet velocity for the portion of the jet acting as a lifting surface. This boundary condition results in a total of $2\,(n_{outlet})$ number of equations.

4. Kutta boundary condition on the jet upper and lower surfaces in such a way that the flow leaves the jet surface smoothly resulting in the velocities on the top and bottom surface to be finite and equal in magnitude and direction:

$$|V_{t,n1}| = |V_{t,n2}| \tag{14}$$

where $n1$ and $n2$ corresponds to the panels located in the immediate vicinity for the velocity outlet surface as shown in Fig. 3.

5. Equivalent Kutta boundary condition for the velocity inlet surface for ensuring the symmetrical flow distribution over the velocity inlet surface:

$$|V_{t,n3}| = |V_{t,n4}| \tag{15}$$

The tangential velocities on the panels in the immediate upstream of the velocity inlet surface are finite and equal in magnitude and direction.

6. Tangential velocity boundary condition for ensuring a smooth transition between (base aerofoil, lower jet.) and (nacelle aerofoil and upper jet surface):

$$V_{t,n5} = V_{t,n6} \tag{16}$$

$$V_{t,n6} = V_{t,n8} \tag{17}$$

where $n5$, $n6$, $n7$ and $n8$ correspond to panels in the immediate vicinity of the surface intersection points ($P1$, $P2$) as shown in the Fig. 3.

The boundary conditions 9 to 17 results in the formation of a system of equations of size,

$$EQN_{count} = n_{lower} + n_{base} + n_{nacelle} + n_{upper} + 2(n_{outlet} + n_{inlet}) + 4 = VAR_{count} \tag{18}$$

This system can be linearised in terms of the unknown variables of the system and can be solved using conventional matrix inversion algorithms.

3.3 Propulsor Characterisation

To correlate the jet speed to the power added to the flow by the fan, a simple propulsor assembly is modelled. It is composed of an inlet, a fan in a duct and a nozzle, with no information included on power source component (e.g. electric motor in a distributed propulsion configuration). A 0D thermodynamic model of the fan is developed using the well-established conventional jet engine modelling approach as described in e.g. [10], using the standard station numbering (Fig.4).

The propulsor performance is characterized using the following inputs:

1. Fan power setting, ($\mathscr{P}$)
2. Fan isentropic efficiency, (η_{is})
3. Nozzle static pressure condition. (P_{s9})

Once flight operating conditions, fan performance inputs and heat (adiabatic) and pressure loss assumptions are specified, fluid state in terms of pressures and temperatures at different stations can be calculated by correlating the fan power to the enthalpy and total temperature

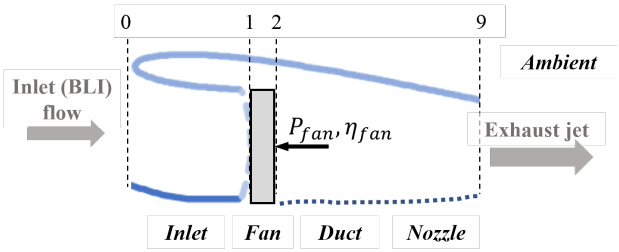

Figure 4: Schematic overview of the propulsor assembly model with the employed station numbering.

and using it to find the fan pressure ratio via the fan efficiency. With the resulting temperatures and pressures, and using the adapted nozzle hypothesis, the resulting speeds and propulsor thrust can be deduced. To complete the information, the mass flow rate passing through the adiabatic fan and the perfectly expanded nozzle needs to be iterated upon. The iterations start with an initial guess on the mass flow rate ($\dot{m}_1$) at the fan inlet station. With this initial mass flow rate estimate and fan performance inputs, the thermodynamic properties at different stations are evaluated using the standard 0D thermodynamic approach as described above. Once the conditions at the nozzle exit (station 9) are calculated, it allows to deduce the local mass flow using the continuity equation. This result is compared with the initial mass flow rate guess; since no additional mass is added to the system the mass flow rate must be constant thoughout the propulsor. Depending upon the difference between the initial guess ($\dot{m}_{guess,1}$) and the calculated ($\dot{m}_9$), the initial guess is corrected and the process is iterated until a convergence between the two mass flow rates is obtained.

After a mass flow rate convergence is obtained ($\dot{m}_1 = \dot{m}_{conv,1}$), the velocity at the station 1 can be finally determined using the same system of equations, in summary:

$$\dot{m}_{conv,1} = \frac{P_{t1}}{\sqrt{T_{t1}}} area_1 \left(\frac{\gamma}{r_g}\right)^{0.5} M_1 \left(1 + \frac{\gamma - 1}{2} M_1^2\right)^{-\frac{\gamma+1}{2(\gamma-1)}}$$

$$T_{s1} = \frac{T_{t1}}{\left(1 + \frac{\gamma-1}{2} M_1^2\right)} \quad P_{s1} = P_{t1} \left(\frac{T_{s1}}{T_{t1}}\right)^{\frac{\gamma}{\gamma-1}} \quad \rho_1 = \frac{P_{s1}}{r_g T_{s1}}$$

$$V_1 = \frac{\dot{m}_{conv,1}}{\rho_1 area_1} \tag{19}$$

Finally, the velocities evaluated at the station 1 and station 9 can be used as boundary conditions in the panel method (Eqs. 10, 12 and 13) for calculation of vorticity and source strength distributions over different panels of the aero-propulsive element.

NB: as there is no boundary layer modelling in this first approach it justifies modelling of the propulsor as if it were in isolation, i.e. without any inlet flow distortions

and the related mass flow deficit. This will be improved upon in the future development.

3.4 Algorithm for Jet Shape Determination

Aerodynamic advantages of the aero-propulsive element under consideration are significant due to the presence of the jet element. A high lift is not only achieved due to the vertical component of the jet momentum but also due to the additional pressure lift created by the aerofoil which arises from the asymmetry created in the main stream due to the presence of jet. In the current study, as mentioned earlier the portion of the jet exhaust with a constant total pressure acts as a lifting surface and the shape taken by the exhaust jet in the free field is critical in deciding the asymetricity introduced by the flow field and increasing the lift of the configuration.

The shape of the jet is defined using the nomenclature defined in the Fig. 3 in a free stream with a flow at velocity V_∞ with an angle of attack α, using the following variables:

1. Jet depth of penetration (L_{dop}),
2. Total length of the jet (L_T),
3. Jet exhaust angle (θ),
4. Jet asymptote angle at the trailing edge (θ_1),
5. Jet thickness (t_{jet}),
6. Control Point 1: Point of the jet emanation (x_1, y_1),
7. Control Point 2: Point of jet diffusion (x_2, y_2).

The shape of the jet is determined using the following criteria:

1. The jet shape is assumed to be cubic function-shaped;
2. The depth of penetration of the jet (L_{dop}) is evaluated such that the vertical component of the thrust developed at the fan nozzle outlet balance the integrated vertical pressure force on the free jet;
3. The length of the jet (L_T) is extended until the integrated vertical component of the force on the last 5% of the jet is negligible for a chosen jet asymptote angle (θ_1);
4. A low degree of spatial variation between the control point 2 position obtained from the (L_{dop}, L_T) pair obtained via the previous two criteria and the control point 2 position obtained from the pressure fields developed over the jet surfaces.

Starting with an initial guess on (L_{dop}, L_T) pair, defined jet exhaust angle (θ) and jet asymptote angle (θ_1), the shape of the jet is defined as:

$$f_{jet}(x) = ax^3 + bx^2 + cx + d \tag{20}$$

and the four coefficients a, b, c, d in the jet shape function (f_{jet}) are determined using the following boundary conditions:

1. Control point 1 position ($f_{jet}(x_1) = y_1$),
2. Control point 2 position ($f_{jet}(x_2) = y_2$),
3. Slope of the jet at control point 1 ($f'_{jet}(x1) = \tan(\theta)$),
4. Slope of the jet at control point 2 ($f'_{jet}(x2) = \tan(\theta_1)$.

Independent of the cubic shape assumption of the jet, the location of the control point of the jet can also be calculated from the pressure fields developed over its surfaces, in such a way that the centrifugal forces developed due to the radius of curvature of the jet are balanced by the developed pressure fields over the jet. As described by Herold [11], after the division of the exhaust jet into several small polar elements, the author derived the change in polar element jet angles ($\phi - \phi^*$) for a single polar element in terms of pressure differential across the element ($P_{s1} - P_{s2}$) using radial force balance equations and irrotational flow assumptions for the jet exhaust flow as

$$\phi = \phi^* + 2\arcsin\left(\frac{2\rho_{jet} t_{jet} V_{jet}^2}{a(P_{s1} - P_{s2})}\right) \tag{21}$$

At any given operating condition, after the jet is discretised into several smaller polar elements, using the Eq. 21, the variation in jet angle (ϕ) can be evaluated for each discrete polar element of the jet. These evaluated jet angles can be utilised reconstruct the shape of the jet and re-evaluate the position of the control point 2 (point of jet diffusion). Under the fourth criterion of the jet shape determination algorithm, the spatial variation between the control point 2 evaluated using the developed pressure fields and the control point 2 evaluated using the second and third criterion should be minimal.

4. BASE CASE RESULTS

4.1 Base Case Description

The verification of the developed panel code method has been performed against at the similar operating and geometric configurations of the aero-propulsive assembly considered by Benichou et.al [3] for evaluating the impact of BLI propulsion on airplane aerodynamic performance. The properties of the aero-propulsive configuration base case are considered as follows: free-field conditions ($P_\infty, M_\infty, T_\infty, \alpha$): (101325 Pa, 0.11, 288.15K, 0°), configuration geometric properties: base aerofoil: ms0313, nacelle aerofoil: NACA0012, c_{base}: 2.0m, $c_{nacelle}$: 0.84m, nacelle LE (x,y): (0.927m, 0.466m), nacelle relative twist angle (τ): $-4.2°$, jet exhaust angle (θ): 5°, jet asymptote angle (θ_1): 5°, fan power: 123.318 kW, fan isentropic efficiency (η_{is}): 0.84.

4.1.1 Aero-propulsive element RANS model

A 3D CFD Reynolds-Averaged Navier-Stokes (RANS) simulation was provided for validation purposes. The

CFD case consists in the model of an aero-propulsive system assessing a BLI configuration. To that end, the model employs a Body-Force Modelling approach to simulate the propulsor operation. The 3D model of the aero-propulsive system is meshed using an unstructured mesh approach for both volume and surface summing up more than 17.3 millions cells through the whole domain. The RANS CFD case was set to simulate the aero-propulsive system at take off conditions, i.e. at Mach number of 0.11 and propulsor at full power configuration. The lift coefficient at various angles of attack was extracted after simulation convergence to be directly compared against the panel method tool in order to verify the accuracy of the code. Other physical quantities such as inlet/outlet mass flow, static pressures, velocities and temperatures were also extracted from this RANS CFD case as it would help to further evaluate the code.

4.2 Propulsor Modelling Studies

As explained in the subsection 3.3, the fan performance has been characterised in terms of input power ($\mathscr{P}$, polytropic efficiency (η_{poly}) and nozzle exit plane static pressure (P_{s9}). While the first two parameters are user input, the nozzle exit plane static pressure has to be evaluated from the average static pressure measured from the base and nacelle aerofoil trailing edge, which are highly sensitive to the behaviour of boundary layers on the base and nacelle aerofoils. As the developed inviscid panel method cannot capture the development of boundary layers on the surfaces and potential flow separations at higher angles of attacks, the average static pressure at nozzle exit plane measured from the RANS simulation of the base case and is taken to be constant across different power settings considered in this study. From the data given in Tab. 1, we can draw a conclusion that nozzle exit static pressure is independent of angle of attack for a constant power setting.

Table 1: P_{s9} variation with AOA from the reference RANS simulations.

	0deg	**2deg**	**4deg**	**6deg**	**10deg**
$\dot{m}_1$**(kg/s)**	14.71	14.71	14.71	14.71	14.68
V_9**(m/s)**	177.8	176.2	176.16	176.43	175.68
P_{s9}**(Pa)**	94251	94229	94164	94227	94373

4.3 Panel Size Dependence Study

A panel size dependence study was performed to determine of the mean panel length which ensures the independence of the calculated lift coefficient from the number of panels used to describe the body. 1D panelling of the aero-propulsive element is performed with the help of an open source software GMSH [12]. Panel size is controlled with the help of a factor called h, which is inversely proportional to the number of panels required to describe the surfaces. As seen in Fig. 5, for $h = 0.6$, a satisfactory convergence in lift coefficient is obtained, with a total of 1012 panels required to describe the body. Any further decrease in the factor h leads to a significant increase in the number of panels, which increases the computational intensity without a tangible lift coefficient variation. The observed erratic behaviour is attributed to use of constant step size throughout the convergence study. For the purposes of this preliminary tool verification the result was deemed satisfactory, and a more in-depth analysis will be carried out in the future development of the tool.

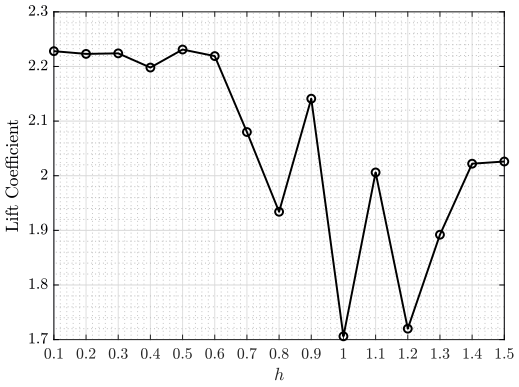

Figure 5: Panel size dependence study, *Cl* convergence.

5. PARAMETRIC STUDIES

A range of parametric studies was carried out to assess the robustness of the developed tool across the design space. A representative sample of possible variation consists of study of angle of attack and jet exhaust angle influence, airframe parameter influence and the propulsive power influence, each presented in their respective subsections below.

5.1 Lift Coefficient Sensitivity to Angle of Attack (α) and Jet Exhaust Angle (θ)

Example parametric studies are performed, as function of angle of attack α and jet exhaust angle θ. The results (Fig. 6) indicate a linear variation in lift coefficient (Cl) with α, with slope of 0.254 deg^{-1}. Moreover, with increasing α, the depth of penetration of the jet also increases linearly with a slope of 0.076 deg^{-1}. A linear relationship between α and Cl is expected because the sources responsible for the introduction on non-linearity in the relationship, mainly the flow separation due to development of a boundary layer on the aerofoil surfaces, are not modelled in this inviscid panel code method.

Fig. 7 presents the calculated linear relationship between the jet exhaust angle variation and Cl at a constant α with a slope of 0.143 deg^{-1}. It can be inferred from the analysis that Cl of this configuration is more sensitive to changes in α rather than the θ. An increase in Cl is expected with increasing θ because at higher exhaust angles, the vertical component of the jet reaction force increases, combined with an increase in curvature of the equivalent aero-propulsive element.

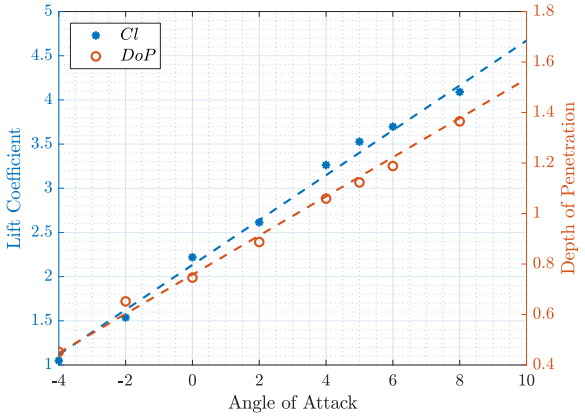

Figure 6: Lift coefficient and jet depth of penetration variation with angle of attack.

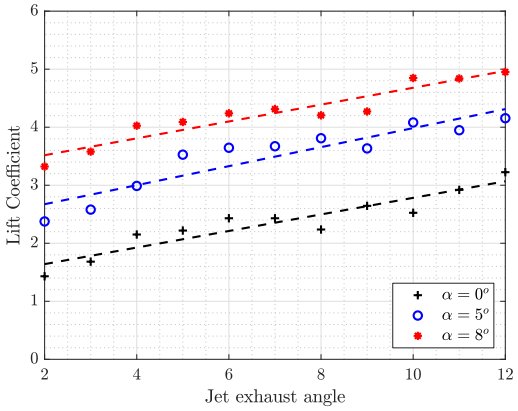

Figure 7: Lift coefficient variation with the jet exhaust angle.

5.2 Airframe Parametric Studies

For understanding the effect of the base and nacelle aerofoil geometry variations on the total lift generated by the aero-propulsive element, 2 geometric parametric studies are presented (Fig. 8).

5.2.1 Nacelle twist angle variation

Variation in the relative twist of the nacelle aerofoil with respect to base has an inflection point at the relative twist of $-4.2°$ (base case) (Fig. 8(a)). A negative nacelle aerofoil twist corresponds to a situation where the nacelle aerofoil is at higher angle of attack compared to the base aerofoil. A clear increase in Cl is observed for small relative angle of attacks, as the lift generated by nacelle aerofoil increases. But a higher relative twist results in the stagnation point to move downstream on the suction side of the nacelle aerofoil resulting in a decrease in nacelle lift and hence the overall configuration lift.

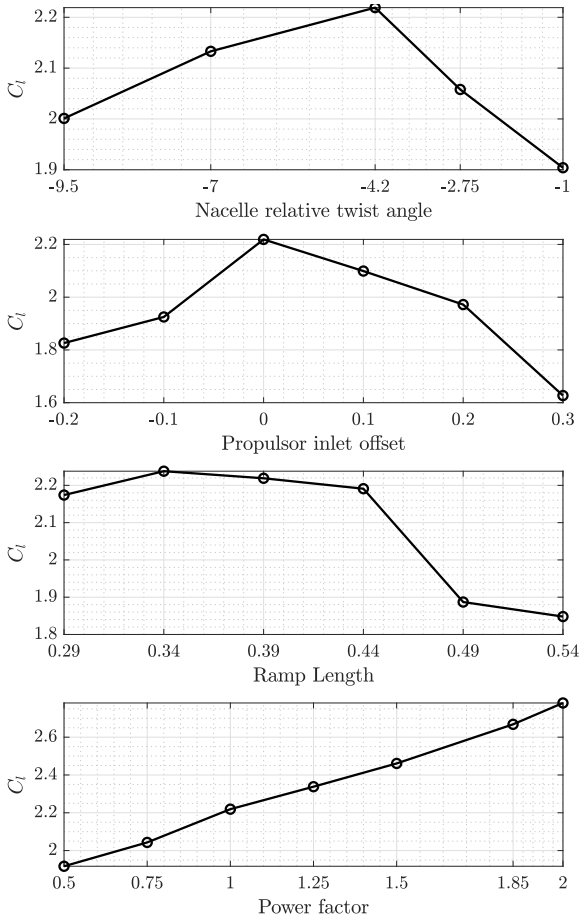

Figure 8: Lift coefficient variation for different propulsor parameters.

5.2.2 Propulsor inlet ramp length variation

The inlet ramp of the current aero-propulsive configuration is defined as a concave surface (Fig. 3). As the flow follows the shape of the body, a low pressure region is created at the start of the ramp when the flow turns. But downstream, as the flow has to follow a concave surface, a region of adverse pressure gradient is created on the concave surface of the ramp. So as seen from the Figure 8(c), smaller ramp lengths have a similar total lift as the lift gain due to low pressure region is balanced by the adverse pressure gradient formed. However, if the length

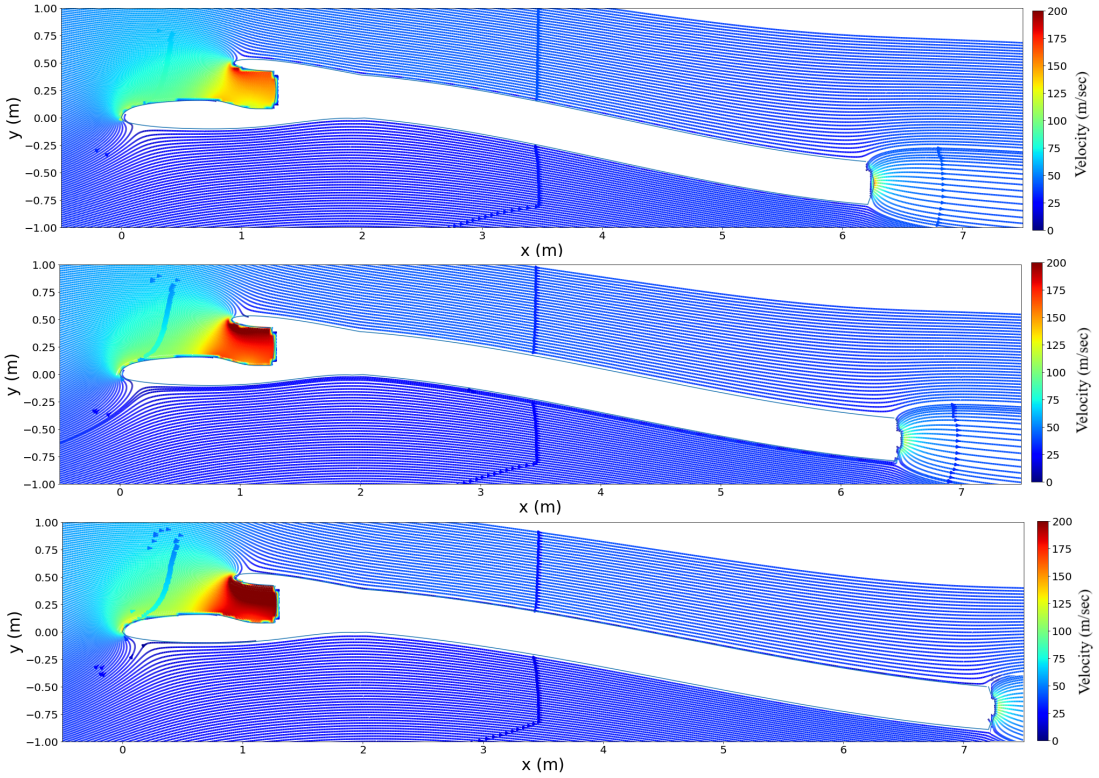

Figure 9: Velocity field at $\alpha = 0°$ at 75%, 100% and 150% power respectively.

of the ramp increases, the drop in lift will be significant due to a significantly longer portion of ramp surface being exposed to adverse pressure gradient. For this reason, the results presented in Fig. 8(c) indicate a precipitous drop in lift for longer ramp lengths.

5.3 Propulsor Power Parametric Study

The variation in lift coefficient with propulsor power is shown in the Fig. 8(d). Power factor corresponds to the ratio between the study case fan power and base case fan power (i.e. 123.3 kW). With an increasing fan power, the nozzle exhaust velocity (V_9) increases, which increases the magnitude of reaction in the force balance criterion of jet shape algorithm. This will ultimately result an increase in Cl as observed in Fig. 8(d). Variation in static pressure and velocity fields with increasing fan power can also be observed (Figs. 10 and 9 respectively).

5.4 Pseudo-Validation with RANS CFD Simulations

Since no experimental setup is available at the moment, the authors resorted to a pseudo-validation of the tool results by comparing it to a limited set of data available from previous 3D RANS BFM CFD simulations [3]. Fig. 11 presents the respective lift coefficient results obtained from RANS CFD simulations and the panel method tool. At low angles of attack, the tool shows a relatively close agreement with the RANS CFD results. However, as the angle of attack increases, the gap between both numerical methods also increases. This was expected as the panel code solves only for the inviscid Euler equations whereas the RANS CFD simulation includes a viscous model to model the non-linearity effects introduced by the boundary layer development over the airfoil surfaces by modelling the entire spectrum of turbulent eddies using an $k-\omega$ SST turbulence model. It is reassuring that the results are of the same order of magnitude between the two, and futher efforts will concentrate on comparing the results across the broader design space in order to ascertain the potential for calibration of the developed tool.

6. CONCLUSIONS

The presented work is a first step in developing a low-order tool dedicated to capturing performance trends of a two-dimensional aero-propulsive system across large design space. Panel method was chosen to this purpose in order to leverage the robustness and efficiency traditionally associated to it, indispensable in conceptual design. The aero-propulsive system is defined by considering the airframe, the propulsor and the emanating jet as a single

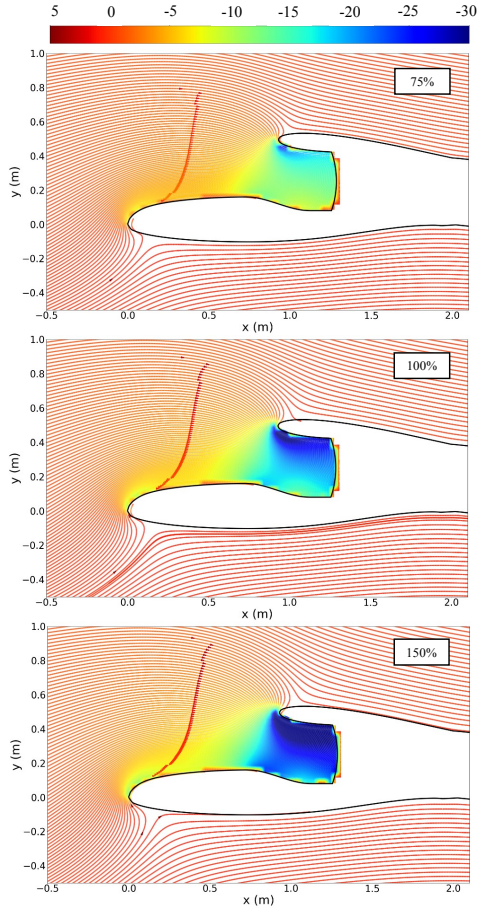

Figure 10: Static pressure field at $\alpha = 0^\circ$ at 75%, 100% and 150% power respectively.

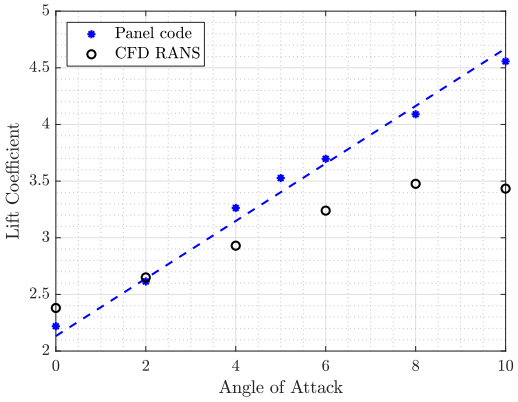

Figure 11: comparison of the lift coefficient obtained with the developed panel method and reference RANS CFD simulations.

aerodynamic solid body in the panel code; the operating setting of the propulsor (i.e. its power) is correlated to the size and shape of jet, which influences the overall pressure field around the complex body. This is enabled by implementing a thermodynamic 0D model into the tool to characterise the propulsor performance along with an algorithm to determine the jet shape.

Results of the performed studies indicate that the code is able to determine the two dimensional potential flow solution for the defined aero-propulsive configuration and the shape of exhaust jet; for the moment, all calculations were carried out for a single flight condition representative of takeoff for a small commuter aeroplane. Parametric studies have been performed to verify the performance of the developed panel method tool at various off-design operating conditions. Finally, a comparison was made between the lift coefficients calculated with the developed panel method and a RANS CFD solver. A satisfactory match of the results was observed at lower angles of attack, but not at higher angles of attack, likely due to the inherent limitation of the employed inviscid model.

6.1 Ongoing and Further Work

Currently, a development of viscous-inviscid coupling is ongoing. The pressure and the velocity distributions around the aero-propulsive configuration obtained from this potential flow solution can be used to characterize the boundary layer growth and flow separations on different surfaces of the aerofoils. With the help of such a coupling, a more robust 0D thermodynamic model can be designed which directly uses the static pressure fields at the nacelle trailing edge as fan exit nozzle static pressure. From boundary layer parameters like displacement and the momentum thickness, estimates of skin friction factors can be obtained which could be used for determining an optimal location and orientation of propulsive systems for various operating conditions, which can be integrated in overall aircraft design processes. This could render aircraft-level trade-offs transparent, which is indispensable if coherent conclusions are to be drawn on energy performance of the innovative architectures that rely on aero-propulsive synergies.

REFERENCES

[1] D. Lee, D. Fahey, A. Skowron, M. Allen, U. Burkhardt, Q. Chen, S. Doherty, S. Freeman, P. Forster, J. Fuglestvedt, A. Gettelman, R. De León, L. Lim, M. Lund, R. Millar, B. Owen, J. Penner, G. Pitari, M. Prather, R. Sausen, and L. Wilcox, "The contribution of global aviation to anthropogenic climate forcing for 2000 to 2018," *Atmospheric Environment*, vol. 244, Jan. 2021.

[2] H. D. Kim, "Distributed propulsion vehicles," in *27TH International Congress of the Aeronautical Sciences*, NASA Glenn Research Center, 2010.

[3] E. Benichou, V. Maillet, A. Joksimović, C. Crabé, and X. Carbonneau, "Numerical low-fidelity

method for improved analysis of breakthrough aero-propulsive systems," in *1st Edition of the Aerospace Europe Conference (AEC2020)*, (Bordeaux, France), 2020.

[4] E. S. Hendricks, "A Review of Boundary Layer Ingestion Modeling Approaches for use in Conceptual Design," Technical Memorandum NASA/TM-2018-219926, NASA Glenn, Cleveland,Ohio,US, 2018.

[5] J. A. Albers and M. C.Potter, "Potential flow solution for a stol wing propulsion system," unclassified, National Aeronautics and Space Administration, July 1971.

[6] D. A. Spence, "The lift coefficient of a thin, jet-flapped wing," *The Royal Society*, vol. (doi: 10.1098/rspa.1956.0203), no. 238, pp. 46–68, 1956.

[7] A. T. Wick, J. R. Hooker, and C. H. Zeune, "Integrated Aerodynamic Benefits of Distributed Propulsion," in *53rd AIAA Aerospace Sciences Meeting*, (Kissimmee, Florida), American Institute of Aeronautics and Astronautics, Jan. 2015.

[8] N. D. Halsey, "Methods for the design and analysis of jet-flapped airfoils," *Journal of aircraft*, vol. 11, pp. 540–546, Sep 1974.

[9] J. Katz and A. Plotkin, *Numerical (Panel) Methods*, p. 206–229. Cambridge Aerospace Series, Cambridge University Press, 2 ed., 2001.

[10] J. D. Mattingly, *Aircraft Engine Design, Second Edition*. Reston ,VA: American Institute of Aeronautics and Astronautics, Jan. 2002.

[11] A. Herold, "A two-dimensional, iterative solution for the jet flap," 1973.

[12] C. Geuzaine and J.-F. Remacle, "A three-dimensional finite element mesh generator with built-in pre- and post-processing facilities," *International Journal for Numerical Methods in Engineering*, no. J, pp. 1–24, 2009.